Drastically enhanced hydrogen evolution activity by 2D to 3D structural transition in anion-engineered molybdenum disulfide thin films for efficient Si-based water splitting photocathodes

Supplementary Information

Ki Chang Kwon,[†a,b] Seokhoon Choi,[†a] Joohee Lee,[b] Kootak Hong,[a] Woonbae Sohn,[a] Dinsefa Mensur Andoshe,[a] Kyoung Soon Choi,[c] Younghye Kim,[a] Seungwu Han,[a] Soo Young Kim,[*b] and Ho Won Jang[*a]

[a] Department of Materials Science and Engineering, Research Institute of Advanced Materials, Seoul National University, Seoul 08826, Republic of Korea

[b] School of Chemical Engineering and Materials Science, Chung-Ang University, Seoul 06974, Republic of Korea.

[c] Advanced Nano Surface Research Group, Korea Basic Science Institute, Daejeon 34133, Republic of Korea.

* Corresponding authors, E-mail: Soo Young Kim: sooyoungkim@cau.ac.kr,

E-mail: Ho Won Jang: hwjang@snu.ac.kr

† These authors contributed equally to this work.
* These corresponding authors contributed equally to this work.

Fig. S1. Optical and electrical characterization of synthesized thin films. (a) Transmittance and (b) absorbance spectra of the thin films synthesized with different S/P powder precursor ratios. Transmittance was gradually increased with respect to increase of P mounts. MoS_2 and P:MoS_2 (S/P = 3:1) showed the characteristic absorption peaks of MoS_2. When the phosphorus ratio increased, the MoS_2 absorption peak disappeared, indicating that the phosphorus-rich (S:MoP, S/P =1, S/P = 0.33, and P) thin films were metallic. (c) The current-voltage (I-V) sweep data with 0.1 A compliance. The S:MoP (S/P = 0.33 and P) thin films show the metallic behavior, while the MoS_2 (S) and P:MoS_2 (S/P = 3 and S/P =1) thin films show the semiconducting behavior. (d) The magnified I-V curve of dashed region in the (c). The MoS_2 (S) and P:MoS_2 (S/P = 3) thin films clearly showed the unequal rectifying behavior which means semiconducting property.

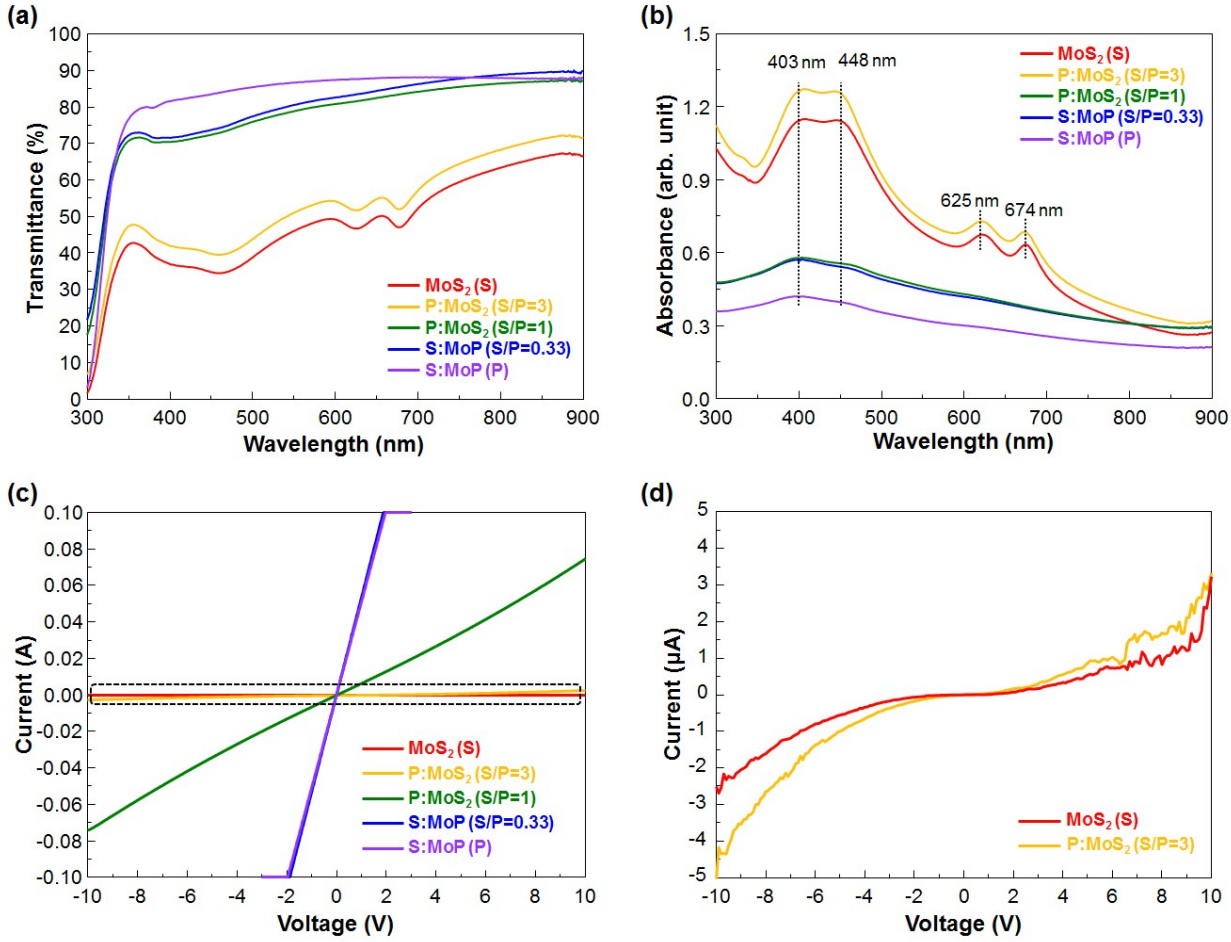

Fig. S2. XPS wide scan of the thin films synthesized with different S/P powder precursor ratios.

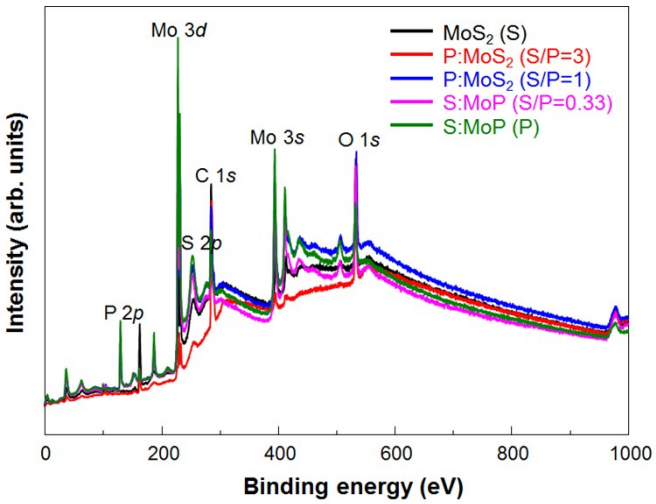

Fig. S3. The XPS atomic ratio of synthesized thin films as a function of the S/P powder precursor ratio.

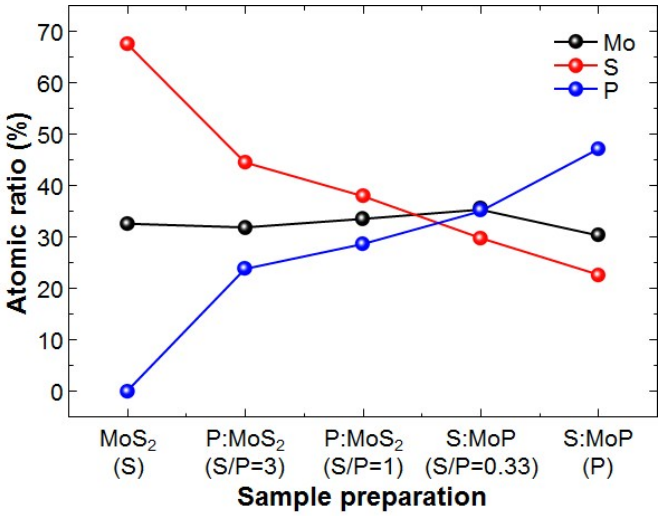

Fig. S4. AFM images of the thin films synthesized with different S/P powder precursor ratios. Nano-granular surfaces were observed in each thin film.

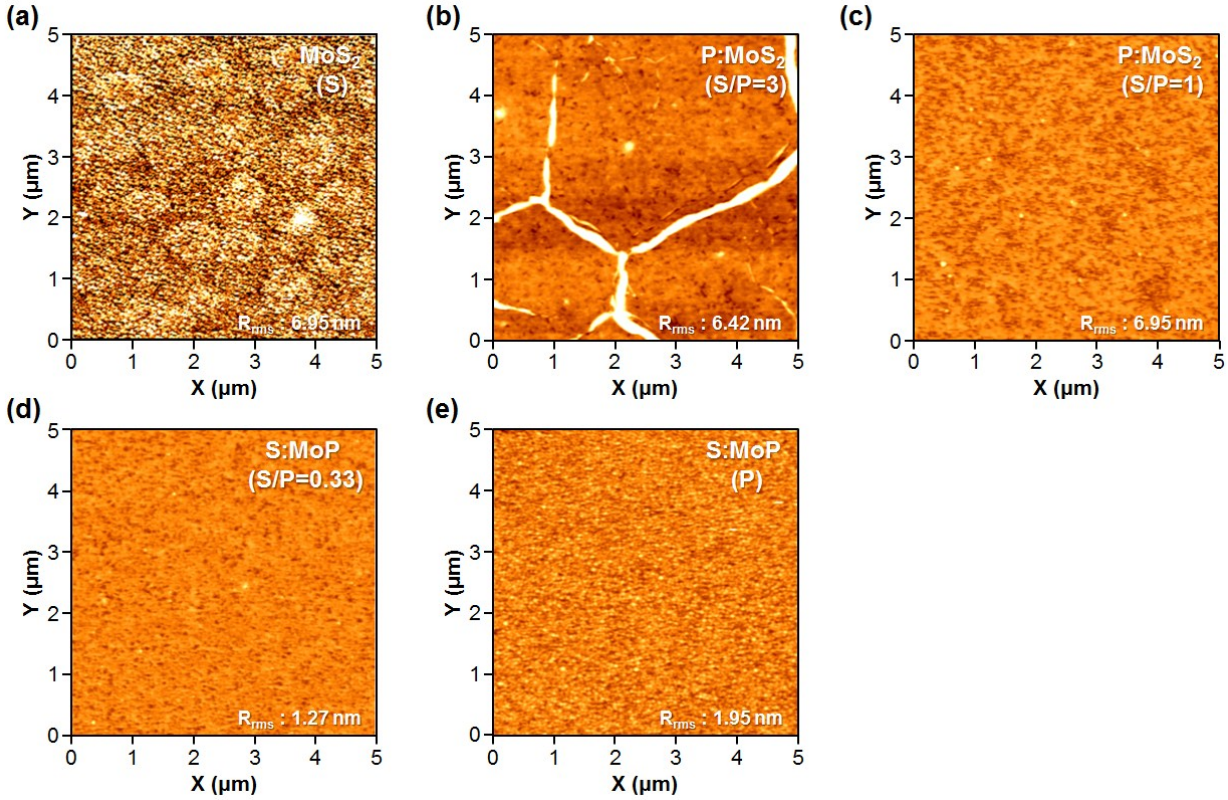

Fig. S5. AFM images with line profiles of the thin films synthesized with different S/P powder precursor ratios. The thickness of the synthesized thin films decreased from ~ 20 to ~ 13 nm when P atoms were completely substituted into the MoS_2 atomic structure.

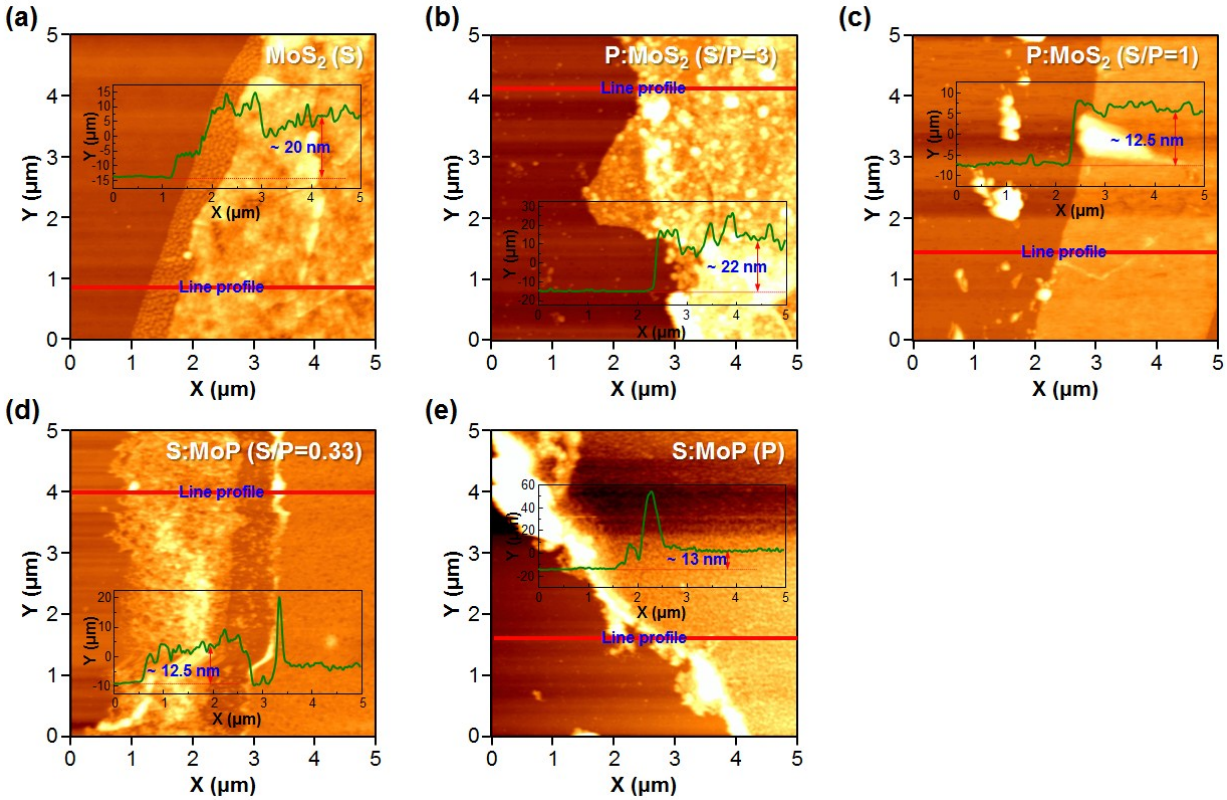

Fig. S6. Surface analysis of synthesized thin films with 5 different regions. The average RMS roughness values of MoS_2 and S:MoP (S/P=0.33) are 4.74 and 2.21 nm, respectively.

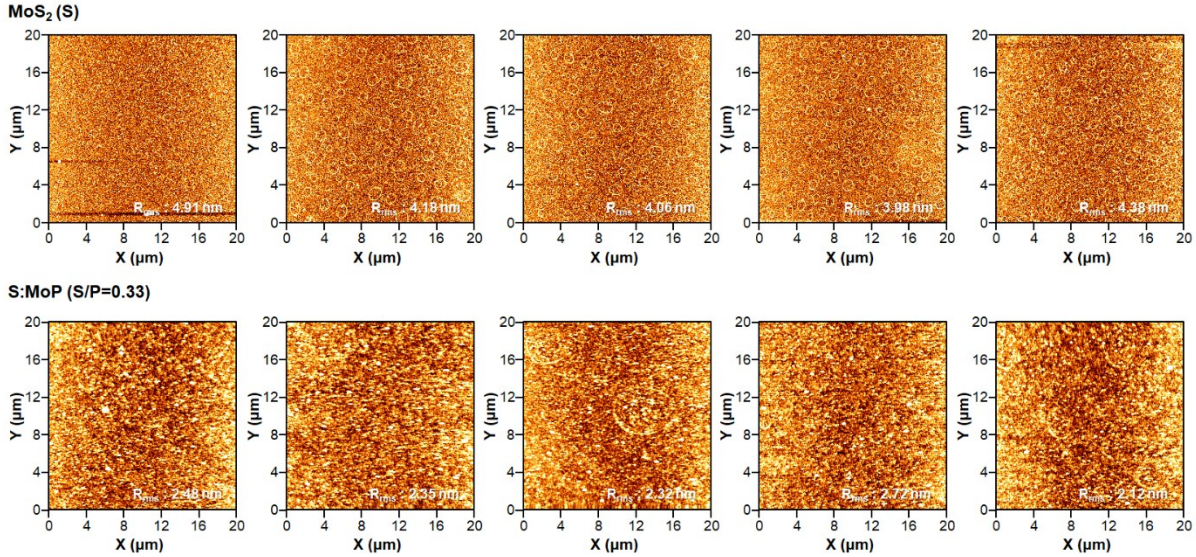

Fig. S7. (a)–(c) The low-magnification transmission electron microscopy (TEM) images of the thin films synthesized with different S/P powder precursor ratios. (d)–(f) The selected area electron diffraction (SAED) patterns of the thin films synthesized with different S/P powder precursor ratios. The SAED patterns of the MoS_2 thin films showed the MoS_2 (002) plane. The SAED patterns significantly changed into MoP (100) and MoP (001) planes with the introduction of phosphorus into the MoS_2 atomic structure.

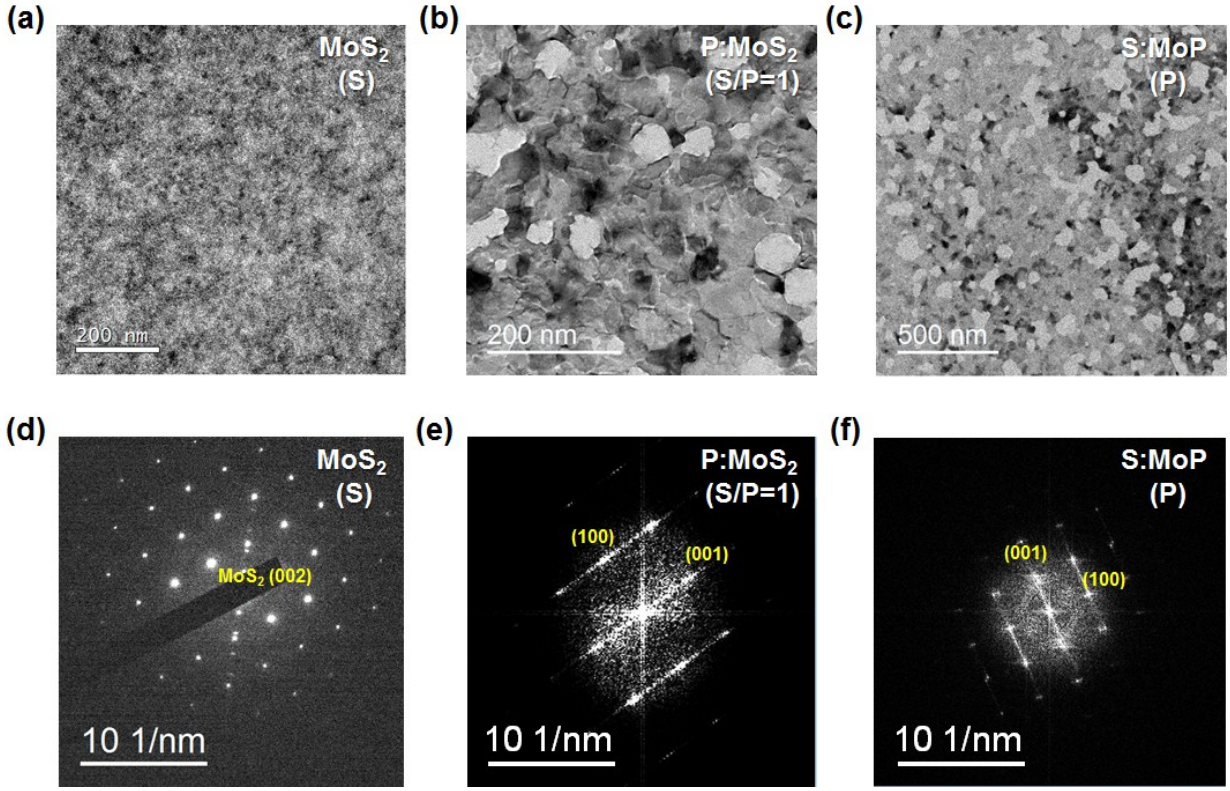

Fig. S8. The high-resolution TEM images of the thin films synthesized with different S/P powder precursor ratios. The surface of the thin films was gradually smoothed with an increase in the S/P powder precursor ratio.

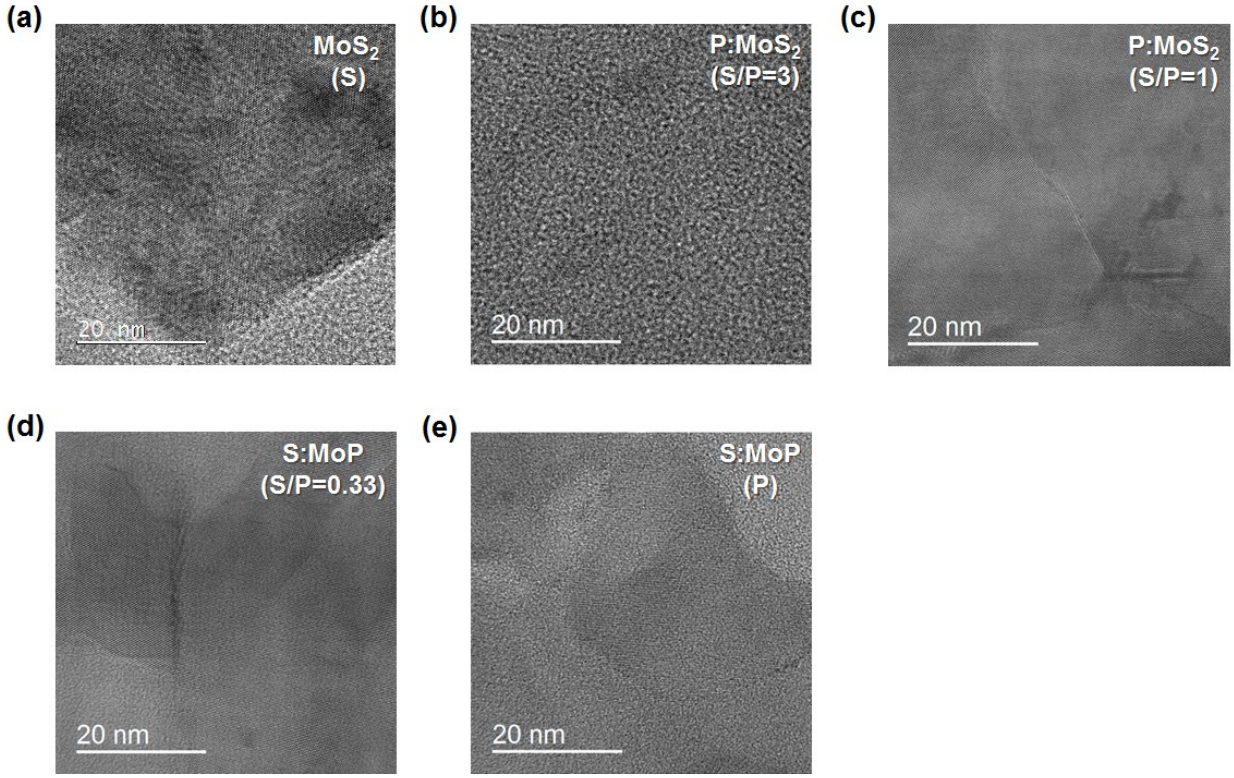

Fig. S9. (a) Electrochemical (EC) performances of the synthesized thin films on Au electrode. (b) Tafel plots from the linear portion of the EC measurement. (c) The electrochemical impedance spectroscopy measurements. (d) The faradaic efficiency measurements of the synthesized thin films transferred onto Au electrodes.

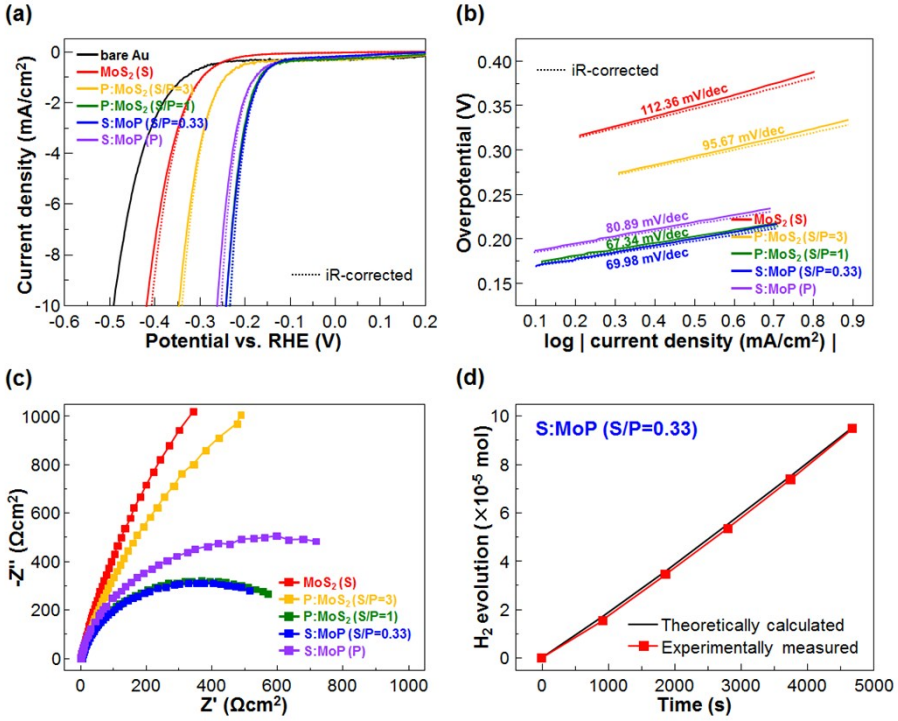

Fig. S10. The cyclic voltammetric curves of (a) MoS_2/*p*-Si and (b) S:MoP (S/P = 0.33)/*p*-Si photocathodes. The statistical results of (c) current density at 0 V, (d) potential vs. RHE @ 10 mA/cm^2, and (e) RMS roughness values for the MoS_2 and S:MoP (S/P = 0.33) thin films.

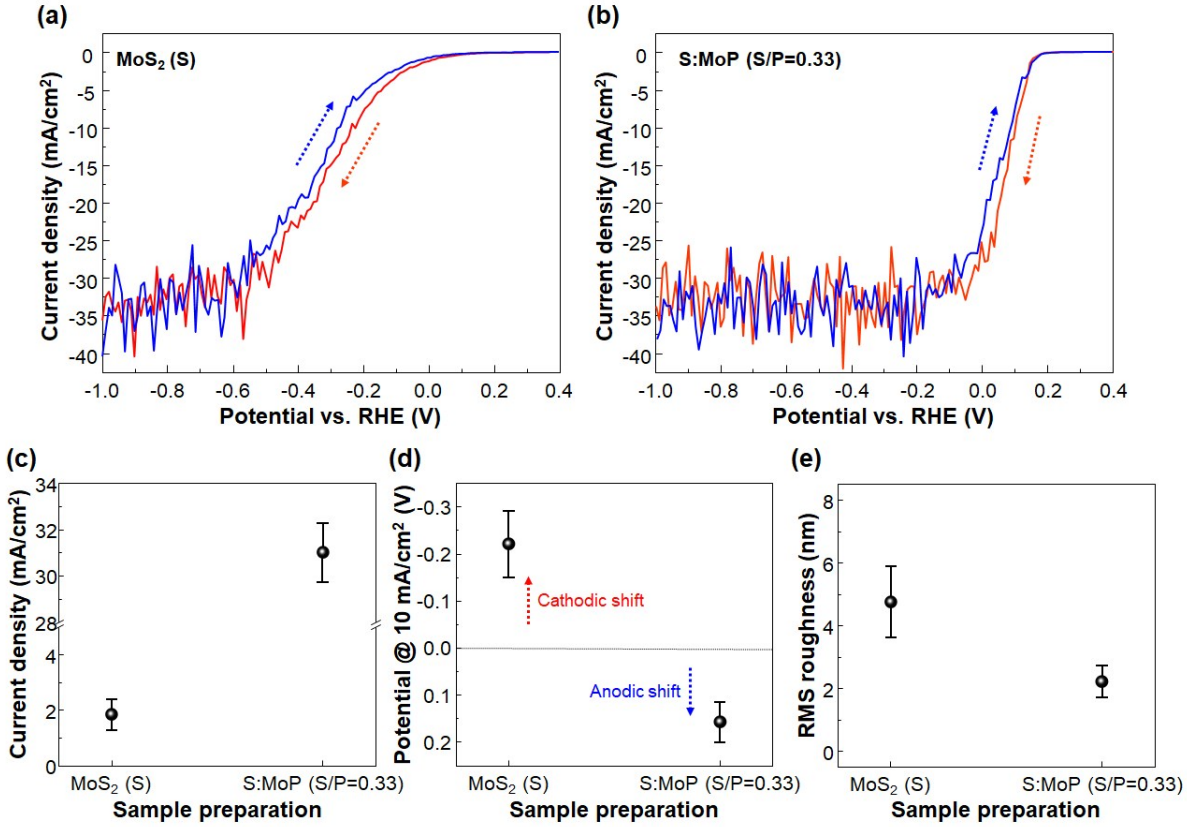

The incident-photon-to-current conversion efficiency spectra of the S:MoP/p-Si were recorded at an applied potential of 0 V vs. RHE, as shown in Supplementary Fig. S11. Among the tested photocathodes, the photocathode with a S:MoP (S/P = 0.33) layer exhibited the highest efficiency of around 80% in the wavelength range of 410–720 nm. The linear-sweep voltammetry curves show that the PEC properties of the S:MoP/p-Si photocathodes depended on the S/P powder precursor ratios and it was necessary to determine an optimum S/P ratio.

Fig. S11. Incident-photon-to-current conversion efficiency measurements of each thin film catalyst/p-Si photocathode.

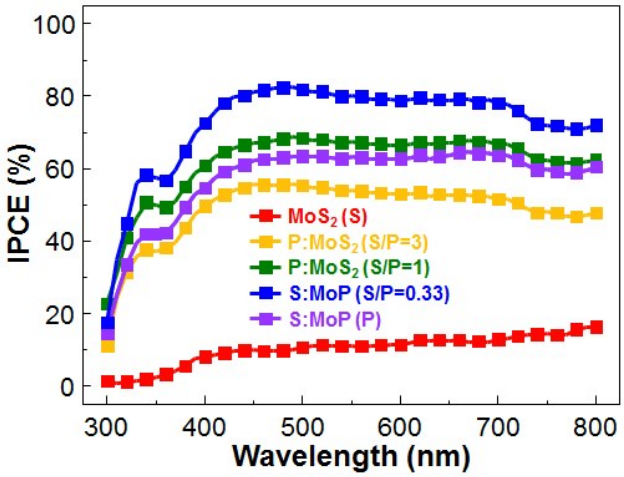

Fig. S12. The flat band and band-banding diagrams of (a) n-MoS_2 (S)/p-Si, and (b) S:MoP (S/P =0.33)/p-Si heterojunction photocathodes.

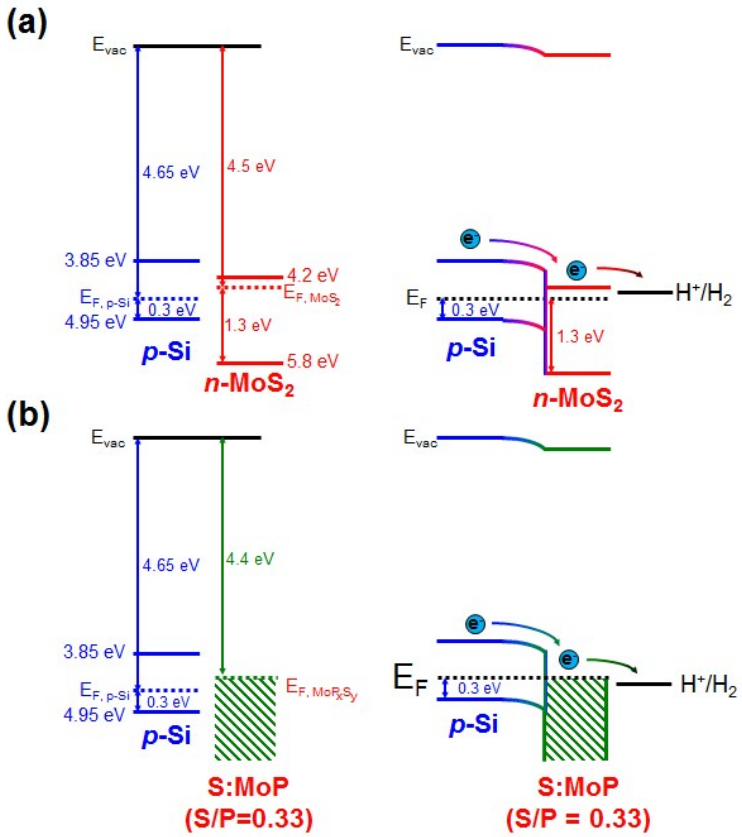

1 **Table S1.** Electrochemical catalytic properties of the thin films synthesized on Au electrodes.
2

Electrodes	Potential (V) @ 10 mA/cm^2	Potential (V) @ 20 mA/cm^2	Tafel slope (mV/dec)
bare Au	- 0.492	- 0.546	157.83
MoS_2 (S)	- 0.407	- 0.450	112.36
P:MoS_2 (S/P=3)	- 0.341	- 0.375	95.67
P:MoS_2 (S/P=1)	- 0.234	- 0.255	67.34
S:MoP (S/P=0.33)	- 0.233	- 0.255	69.98
S:MoP (P)	- 0.254	- 0.276	80.89

Table S2. Electrochemical catalytic properties of the thin films synthesized on Au electrodes.

No.	Sample type	Measured Electrode	Synthesis method	η* at 10 mA/cm^2	Tafel slope (mV/dec)	Ref.
1	grain type	Ti foil	thermal CVD	117 mV	50	1
2	nano-particle	glassy carbon	air ambient calcination	125 mV	54 – 83	2
3	nano-particle	Ti foil	solution-phase synthesis	110 mV	45	3
	porous MoP | S	Ti foil	thermal annealing	90 mV	50	
4	mirco-particle	glassy carbon	grinding	150 mV	56	4
5	sponge (3D)	glassy carbon	solution synthesis	105 mV	126	5
6	$MoS_{2(1-X)}P_X$ solid solution	glassy carbon	MoS_2 + red-P solid solution	150 mV	57	6
7	nanosheets	glassy carbon	hydrothermal	43 mV	34	7
This work	**S:MoP thin film**	**Au** ***p*-Si**	**thermal CVD (thermolysis)**	**233 mV** **- 207 mV**	**70** **32**	**-**

*Overpotential.

Supplementary Information References

1. J. Kibsgaard and T. F. Jaramillo, *Angew. Chem.* **2014**, *126*, 14661.

2. Z. Xing, Q. Liu, A. M. Asiri and X. Sun, *Adv. Mater.* **2014**, *26*, 5702.

3. J. M. McEnaney, J. C. Crompton, J. F. Callejas, E. J. Popczun, A. J. Biacchi, N. S. Lewis and R. E. Schaak, *Chem. Mater.* **2014**, *26*, 4826.

4. T. Wang, K. Du, W. Liu, Z. Zhu, Y. Shao and M. Li, *J. Mater. Chem. A* **2015**, *3*, 4368.

5. C. Deng, F. Ding, X. Li, Y. Guo, W. Ni, H. Yan, K. Sun and Y.-M. Yan, *J. Mater. Chem. A* **2016**, *4*, 59.

6. R. Ye, P. del Angel-Vincente, Y. Liu, M. J. Arellano-Jimenez, Z. Peng, T. Wang, Y. Li, B. I. Yakobson, S.-H. Wei, M. J. Yacaman and J. M. Tour, *Adv. Mater.* **2016**, *28*, 1427.

7. P. Liu, J. Zhu, J. Zhang, P. Xi, K. Tao, D. Gao and D. Xue, *ACS Energy Lett.* **2017**, *2*, 745.